

Physics-constrained Deep Learning for Robust Inverse ECG Modeling

Jianxin Xie and Bing Yao*

Abstract—The rapid developments in advanced sensing and imaging bring about a data-rich environment, facilitating the effective modeling, monitoring, and control of complex systems. For example, the body-sensor network captures multi-channel information pertinent to the electrical activity of the heart (i.e., electrocardiograms (ECG)), which enables medical scientists to monitor and detect abnormal cardiac conditions. However, the high-dimensional sensing data are generally complexly structured and realizing the full data potential depends to a great extent on advanced analytical and predictive methods. This paper presents a physics-constrained deep learning (P-DL) framework for high-dimensional inverse ECG modeling. This method integrates the physical laws of the complex system with the advanced deep learning infrastructure for effective prediction of the system dynamics. The proposed P-DL approach is implemented to solve the inverse ECG model and predict the time-varying distribution of electric potentials in the heart from the ECG data measured by the body-surface sensor network. Experimental results show that the proposed P-DL method significantly outperforms existing methods that are commonly used in current practice.

Note to Practitioners—This article is motivated by the remarkably increasing applications of advanced medical sensing and imaging technique for data-driven disease diagnosis and treatment planning. For instance, body surface potential mapping (BSPM) can be invasively acquired to delineate the spatiotemporal potential distribution on body surface, enabling medical scientists to infer the electrical behavior of the heart (i.e., heart surface potential (HSP)). However, the estimation of HSP is highly sensitive to model uncertainty and BSPM measurement noises. This paper presents a novel physics-constrained deep learning (P-DL) framework by encoding the physics principles into the advanced deep-learning infrastructure for robust HSP prediction. Experimental results demonstrate the extraordinary performance of the proposed P-DL model in handling measurement noises and other uncertainty factors.

Index Terms—Deep Learning, Inverse ECG Modeling, Gaussian process, Active learning

I. INTRODUCTION

The development of cutting-edge medical sensing and imaging technique greatly benefits the modeling of complex dynamic systems and further facilitates effective system monitoring and optimization for smart health. For instance, electrocardiography (ECG) is a widely-used diagnostic tool to investigate and detect abnormal heart conditions. It monitors electrical signals on the torso surface initiated by the electrical depolarization and repolarization of the heart chambers, establishing a spatiotemporal pattern of the cardiac electrical

activity [1]. Effective ECG monitoring systems enable medical scientists to non-invasively access the electrical behavior of the heart by simply measuring the electrical potentials on the body surface. Twelve-lead ECG, one of the most widely-used ECG systems, is implemented by strategically distributing four electrodes on limbs and six on the chest to harvest multi-angle views of the spatiotemporal cardiac electrodynamics [2]. However, traditional ECG systems (e.g., 12-lead ECG, 3-lead VCG) only employ a limited number of ECG sensors on the thorax and thus the resulted cardiac electrical distribution is with low spatial resolution. Accurate diagnosis of heart diseases such as acute ischemia calls upon the high-resolution ECG mapping [3] that is capable of capturing a comprehensive 3D view of the cardiac electrical signals. Thus, body surface potential mapping (BSPM) has been developed by deploying an increased number (i.e., 32-231) of ECG electrodes to record the high-resolution spatiotemporal cardiac electrodynamics projected on the body surface [4]–[7].

Rapid advances in sensing and imaging technologies bring abundant data and provide an unprecedented opportunity for data-driven disease diagnosis and optimal treatment planning [8]–[13]. Realizing the full potential of the sensing and imaging data depends greatly on the development of innovative analytical models. In the human heart system, the ECG signal (or BSPM) describes the spatiotemporal distribution of electric potentials on the body surface, which reflects electrical behaviors of the source, i.e., epicardial potentials. When projecting from the heart to the body surface, the spatiotemporal pattern of the cardiac electrodynamics becomes diminished and blurred, which defies the accurate characterization of local abnormal regions in the heart. Precision cardiology [14], [15] calls for advanced analytical models that can effectively handle the spatiotemporal data structure for the robust prediction of heart-surface electrical signals (i.e., heart-surface potentials (HSP)) from body-surface sensor measurements (i.e., BSPMs). This is also called the inverse ECG problem [6], [16]–[18].

Inverse ECG problem is commonly recognized as ill-conditioned, because a small input noise may cause highly unstable prediction. Great efforts have been made to achieve robust inverse solutions by adding proper spatial or/and temporal regularization [19]–[23]. However, most existing regularization methods (e.g., Tikhonov, L1-norm, or spatiotemporal regularization) focus on exploiting the data structure (i.e., data-driven regularization). Little has been done to integrate the well-established physics model of cardiac electrodynamics (i.e., physics-driven regularization) with advanced machine learning approaches for robust inverse ECG modeling. In order

Jianxin Xie and Bing Yao (*corresponding author: bing.yao@okstate.edu) are with the School of Industrial Engineering and Management, Oklahoma State University, Stillwater, OK 74078 USA.

to further increase the estimation accuracy and robustness, it is imperative to incorporate the physics prior knowledge that can theoretically describe the cardiac electrodynamics into the transformation from BSPM data to heart-surface signals. This paper proposes a novel physics-constrained deep learning (P-DL) framework to solve the inverse ECG problem and achieve a robust estimation of HSP from noisy BSPM data. Specifically, our contributions in the present investigation are as follows:

(1) We propose to integrate the physics prior knowledge of cardiac electrodynamics with advanced deep learning (DL) infrastructures to regularize the inverse ECG solution. The loss function of the neural network is delicately designed to not only satisfactorily match the sensor measurements (i.e., data-driven loss) but also respect the underlying physics principles (i.e., physics-based loss).

(2) The effect of the physics-driven regularization (i.e., the physics-based loss) on the inverse solution will be controlled by introducing a regularization parameter, the value of which will impact the prediction performance. We define a balance metric to effectively evaluate the prediction performance of the proposed P-DL framework given different values of the regularization parameter. We further propose to model the balance metric with Gaussian Process (GP) regression, and actively search for the optimal parameter value using GP upper-confidence-bound (GP-UCB).

We evaluate the performance of the P-DL framework to reconstruct the HSP from BSPM data in a 3D torso-heart geometry. Numerical experiments demonstrate the superior performance of our P-DL approach compared with existing regularization methods, i.e., Tikhonov zero-order, Tikhonov first-order, and spatiotemporal regularization method.

The remainder of this paper is organized as follows: Section II presents the literature review of the inverse ECG problem. Section III introduces the proposed P-DL framework. Section IV shows the numerical experiments of the P-DL method to solve the inverse ECG problem in a 3D torso-heart geometry. Section V concludes the present investigation.

II. LITERATURE REVIEW

A. Inverse ECG Modeling and Regularization

The inverse ECG problem consists in reconstructing the cardiac electrodynamics from body-surface sensor measurements. The ultimate goal of inverse ECG modeling is to enable non-invasive mapping of cardiac electrical activity for optimal diagnosis and characterization of heart disease. It has been widely recognized that inverse ECG problem is ill-posed, the solution of which is sensitive to model uncertainty and measurement noises. Specifically, the relationship between BSPM $\mathbf{y}(s, t)$ with HSP $\mathbf{u}(s, t)$ can be expressed as $\mathbf{y}(s, t) = \mathbf{R}\mathbf{u}(s, t) + \epsilon$, where s and t denotes the spatial and temporal coordinates respectively, and \mathbf{R} is a transfer matrix solved by Divergence Theorem and Green Theorem [18], [24]. However, the rank-deficiency of transfer matrix \mathbf{R} (i.e., $\text{rank}(\mathbf{R}) < \min\{\text{dim}(\mathbf{u}), \text{dim}(\mathbf{y})\}$) and its large condition

number (i.e., $\text{cond}(\mathbf{R} = \|\mathbf{R}\| \|\mathbf{R}^{-1}\|)$) make the estimated HSP $\hat{\mathbf{u}}(s, t)$ very sensitive to the BSPM data $\mathbf{y}(s, t)$. Small fluctuation in BSPMs, i.e., $\Delta\mathbf{y}$, will cause a significant variation $\Delta\hat{\mathbf{u}}$ in $\hat{\mathbf{u}}$ (i.e., $\Delta\hat{\mathbf{u}}/\hat{\mathbf{u}} \simeq \text{cond}(\mathbf{R})\Delta\mathbf{y}/\mathbf{y}$). Therefore, regularizing the inverse ECG model for robust solution is crucially important for understanding the mechanism of cardiac physiology and pathology, further facilitating the accurate disease diagnosis and optimal therapeutic design.

In existing literature, remarkable progress has been made in developing statistical regularization algorithms by exploiting the spatiotemporal data structure to improve the robustness of inverse ECG solution. Among them, Tikhonov method (including zero-order and first-order) is one of the most popular regularization approaches. It minimizes the mean squared error (i.e., residual) from body-heart transformation and penalizes the L_2 norm of inverse HSP solution [6], [25]–[27] to suppress the unreliable component and improve the overall smoothness of the solution. The objective function for Tikhonov regularization is formulated in Eq.(1)

$$\min_{\mathbf{u}(s, t)} \{ \|\mathbf{y}(s, t) - \mathbf{R}\mathbf{u}(s, t)\|_2^2 + \lambda^2 \|\Gamma\mathbf{u}(s, t)\|_2^2 \} \quad (1)$$

where $\|\cdot\|_2$ indicates the L_2 norm, λ is regularization coefficient, and Γ denotes the operator constraining HSP solution $\mathbf{u}(s, t)$, which is an identity matrix for zero-order regularization and a spatial gradient operator for first-order regularization to increase the spatial smoothness of the inverse solution. Another widely-used regularization technique is the L_1 norm-based method including zero-order [26] and first-order [28], [29], which penalizes L_1 norm of inverse HSP solution to encourage the model sparsity and regularity. However, both Tikhonov and L_1 regularization methods only consider the spatial data structures in inverse ECG modeling, but do not effectively incorporate the temporal evolving patterns of the cardiac electrodynamics.

A variety of spatiotemporal regularization methods have been developed to fuse the space-time correlations into the inverse ECG problem for robust estimation of HSP [18]–[22]. For example, Messnarz *et al.* [30] reconstructed the potential distribution on the heart surface by defining a symmetric matrix of spatial gradient to account for the spatial correlation and assuming that cardiac electric potentials are non-decreasing during the depolarization phase to address the temporal correlation. Yao *et al.* [31] has proposed a spatiotemporal regularization algorithm by regularizing both the spatial smoothness and increasing temporal robustness in inverse ECG modeling, the objective function of which is given by Eq. (2)

$$\min_{\mathbf{u}(s, t)} \sum_t \left\{ \|\mathbf{y}(s, t) - \mathbf{R}\mathbf{u}(s, t)\|_2^2 + \lambda_s^2 \|\Gamma\mathbf{u}(s, t)\|_2^2 + \lambda_t^2 \sum_{\tau=t-\omega/2}^{\tau=t+\omega/2} \|\mathbf{u}(s, t) - \mathbf{u}(s, \tau)\|_2^2 \right\} \quad (2)$$

where λ_s and λ_t denote the spatial and temporal regularization parameters respectively, and ω is a time window selected to incorporate the temporal correlation. However, most existing spatiotemporal regularization methods mainly focus on

capturing the statistical correlations between adjacent spatial locations and neighboring time points, and do not incorporate the real physics principle that governs the HSP evolving dynamics over time. Note that Wang *et al.* [21] proposed a physiological-model-constrained inverse ECG approach to reconstruct the cardiac electrical potential. They formulated the cardiac system into a high-dimensional stochastic state-space model and solved the inverse ECG model with the unscented Kalman filter. However, this method involves large matrix operation and may also suffer from the problem of error accumulation over time [21]. Little has been done to develop innovative machine learning approaches that can incorporate the underlying physics law for robust and effective inverse ECG modeling.

B. Deep Neural Networks

Deep Neural Network (DNN) or Deep Learning (DL) has been demonstrated to be a powerful tool as a universal function approximator that is capable of handling a variety of problems with strong nonlinearity and high dimensionality [32]. However, very little has been done to utilize the DNN to solve the inverse ECG problem and predict the HSP. This is due to the fact that traditional DNN algorithms require an extensive amount of data for modeling complex physical or biological systems. Such data are generally sparse and costly to acquire, which makes the traditional DNN lack robustness and fail to converge. For example, the intracardiac electrical signals are often measured by placing electrodes within the heart via cardiac catheters [33], which are of low spatial resolution, expensive to acquire, and incur discomforts to patients. To cope with such limitations, recent techniques have been developed to incorporate the underlying physics laws into the DNN training [34], [35], which has been engaged in solving various problems such as simulating incompressible fluid flow by Navier–Stokes equation [36], [37], elastodynamic problem [38], and heat source layout optimization [39], [40].

As opposed to the traditional DNN modeling, where the mechanism underlying the physics system is generally unknown and has to be learned from the observed data, there exists a vast amount of prior knowledge about the cardiac dynamic system which is characterized by the physics-based differential equations. However, very little has been done to leverage the advanced DNN infrastructure and incorporate the physics-based cardiac model for robust inverse ECG modeling. In this work, we propose a P-DL framework to encode physics-based principles into the DNN to robustly reconstruct the dynamic potential mapping on the heart surface from BSPM. Additionally, we develop an active-learning strategy with GP-UCB to efficiently search for the optimal balance between the physics-based constraints and the data-driven residuals. The proposed method not only efficiently incorporates the body-surface sensing data but also effectively respects the underlying physics law, thereby significantly increasing the robustness and accuracy of the inverse ECG solution.

III. RESEARCH METHODOLOGY

A. Cardiac Electrophysiological Model

Different phenomenological models have been developed to study cardiac electrophysiology and delineate the electrical wave propagation in myocardium [41]–[43]. Here, without loss of generality, we utilize Aliev–Panfilov (AP) model [44] that is widely used in various cardiac research to describe the spatiotemporal evolution of cardiac electrodynamics:

$$\frac{\partial u}{\partial t} = \nabla \cdot (D \nabla u) + ku(u - a)(1 - u) - uv \quad (3)$$

$$\frac{\partial v}{\partial t} = \xi(u, v)(-v - ku(u - a - 1)) \quad (4)$$

$$\mathbf{n} \cdot \nabla u|_{\Gamma_H} = 0 \quad (5)$$

where u denotes the normalized HSP, and v represents the recovery current controlling the local depolarization behavior of the cardiac electric potential. Parameters $\xi(u, v) = e_0 + \mu_1 v / (u + \mu_2)$ describes the coupling between u and v , D is the diffusion conductivity, k is repolarization constant, and a controls the tissue excitability. The value of each parameter for the remainder of this research are set as $a = 0.1$, $D = 10$, $k = 8$, $e_0 = 0.002$, $\mu_1 = \mu_2 = 0.3$ from the documented literature [44]. Note that Eq.(5) represents the boundary condition to guarantee there is no electric current flowing out from the heart, where Γ_H is the heart boundary and \mathbf{n} denotes the surface normal of Γ_H . The electrophysiological model in Eq. (3)-(5) will further be used to constrain the DNN model to achieve a robust and accurate inverse ECG solution.

B. Artificial Neural Networks

Deep learning has increasingly drawn significant attention due to its successful applications in a variety of fields, such as image and character recognition, natural language processing, advanced manufacturing, and computer vision [45]–[49]. Feed-forward fully-connected neural network is the most fundamental architecture, which consists of an input layer, multiple hidden layers and one output layer, and the information passes layer-by-layer in one direction. The value of each neuron in a layer is calculated by the sum of the products of weights and outputs from the previous layer, which is then activated by a specific activation function. The relationship between two neighbor layers, layer-($n - 1$) and layer-(n), is generally described by the following equation:

$$\mathbf{x}_n = \sigma(\mathbf{b}_n + \mathbf{W}_n \mathbf{x}_{n-1}), 1 < n \leq k \quad (6)$$

where $\sigma(\cdot)$ represents the active function, k is the total number of layers, \mathbf{W}_n and \mathbf{b}_n are the weight matrix and bias vector for layer-(n) respectively, and \mathbf{x}_n and \mathbf{x}_{n-1} denote the outputs of the ($n - 1$)-th and (n)-th layers, respectively.

Our objective is to solve the inverse ECG problem for the spatiotemporal HSP $\mathbf{u}(s, t)$ through the DNN modeling. The selection of optimal neural network structure will be introduced in IV-A. The hyperbolic tangent function is chosen as an activation function due to its great training performance in multiple-layer neural networks. Here, we implement the basic neural network structure with a tailored loss function that

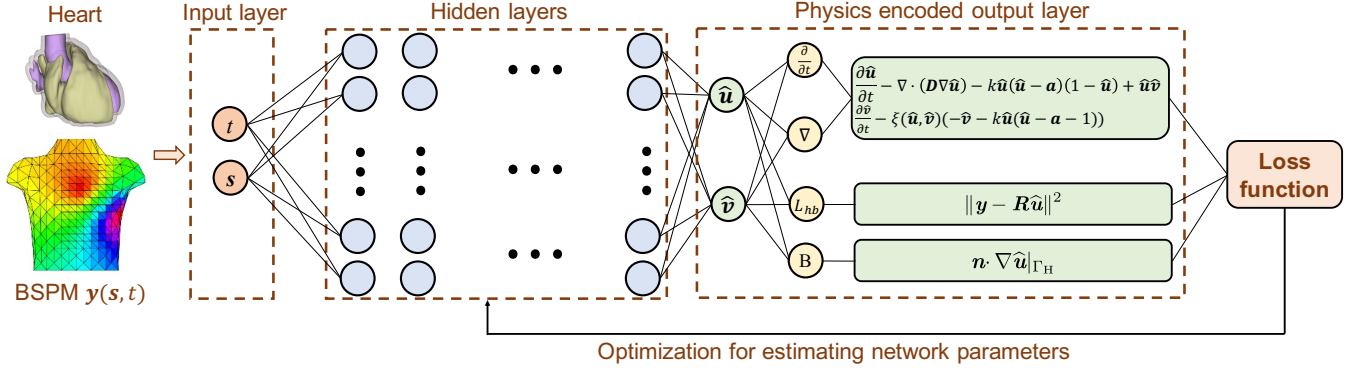


Fig. 1: Illustration of the proposed P-DL framework for HSP prediction. Note that \hat{u} and \hat{v} are the predicted HSP and recovery current, respectively. The physical constraint of AP model and boundary condition are converted into residuals as physical loss \mathcal{L}_{ph} and added to the total loss function of the DNN for respecting the underlying physics principle.

is constrained by the physics law (see Eq. (3)-(5)) to solve the inverse ECG problem, and eventually to obtain the electrical signals on the heart surface. The detailed construction of the P-DL framework will be presented in the following subsection.

C. P-DL approach

Fig. 1 shows the proposed P-DL framework. The solution of the inverse ECG problem is parameterized by a DNN that is trained to not only satisfy the physics law but also meet the data-driven constraint incurred by the body-surface sensor measurements (i.e., BSPM). Specifically, we estimate the spatiotemporal mapping of HSP as

$$[s, t] \xrightarrow{\mathcal{N}(s, t; \theta_{NN})} [u(s, t), v(s, t)] \quad (7)$$

where $\mathcal{N}(s, t; \theta_{NN})$ defines the DNN model, s and t denotes the spatial and temporal coordinates respectively, and θ_{NN} represents the DNN hyper-parameters. Note that the DNN, i.e., $\mathcal{N}(s, t; \theta_{NN})$, is constructed with an input layer composed of the spatiotemporal coordinates $[s, t]$, the hidden layers to approximate the complex functional relationship, and the output layer with the estimation of $\hat{u}(s, t; \theta_{NN})$ and $\hat{v}(s, t; \theta_{NN})$. We further encode the physics law into the DNN by defining a unique loss function as

$$\mathcal{L}(\theta_{NN}) = \mathcal{L}_{hb} + w \cdot \mathcal{L}_{ph} \quad (8)$$

where w is introduced to control the regularization effect imposed by the physics principle. The total loss $\mathcal{L}(\theta_{NN})$ consists of the following two key elements:

(1) **Data-driven loss \mathcal{L}_{hb}** : BSPMs provide the evolving dynamics of electrical potential distribution $y(s, t)$ on the torso surface, which can be leveraged to estimate the heart-surface electrical signals. In human-body system, the heart stands for the bio-electric source and the torso is treated as an electrical volume conductor. The HSP $u(s, t)$ and BSP $y(s, t)$ can be related by the transfer matrix \mathbf{R} (i.e., $y(s, t) = \mathbf{R}u(s, t)$), which is derived according to the divergence theorem and Green's theorem (see more details at [18], [24]). The data-

driven loss generated from the transformation between BSP and HSP, denoted as \mathcal{L}_{hb} , is thus defined as:

$$\mathcal{L}_{hb} = \sum_t \sum_s \|y(s, t) - \mathbf{R}\hat{u}(s, t)\|^2 \quad (9)$$

As stated before, due to the large condition number of the matrix \mathbf{R} , the prediction of HSP lacks accuracy if only minimizing the mean squared error (i.e., training the DNN with only \mathcal{L}_{hb}) without any regularization. Additional constraint needs to be imposed to regularize the DNN-based estimation for robust inverse ECG modeling.

(2) **Physics-based loss \mathcal{L}_{ph}** : In order to further increase the estimation accuracy and robustness, physics constraints are imposed over the spatiotemporal collocation points, $[s_i, t_i]$'s, that are randomly selected within the spatial domain defined by the heart geometry and the temporal domain defined by the cardiac cycle. The physics constraints include two parts: the boundary condition and cardiac electrophysiological model (see Eq. (3)-(5)). Specifically, we define the boundary condition-based residual as:

$$r_{bc}(s, t; \theta_{NN}) := \mathbf{n} \cdot \nabla \hat{u}(s, t; \theta_{NN}), \quad s \in \Gamma_H \quad (10)$$

The boundary condition will then be achieved by encouraging $r_{bc}(s, t; \theta_{NN})$ to be close to zero. As such, we define the boundary condition-based loss as

$$\mathcal{L}_{bc} = \frac{1}{N_{bc}} \sum_{i=1}^{N_{bc}} (r_{bc}(s_i, t_i; \theta_{NN}))^2, \quad s_i \in \Gamma_H \quad (11)$$

where N_{bc} denotes the number of collocation points selected on Γ_H . Additionally, the electrophysiological model-based residuals are defined as

$$\begin{aligned} r_u(s, t; \theta_{NN}) &:= \frac{\partial \hat{u}}{\partial t} - \nabla \cdot (D \nabla \hat{u}) - k \hat{u}(\hat{u} - a)(1 - \hat{u}) + \hat{u} \hat{v} \\ r_v(s, t; \theta_{NN}) &:= \frac{\partial \hat{v}}{\partial t} - \xi(\hat{u}, \hat{v})(-\hat{v} - k \hat{u}(\hat{u} - a - 1)) \end{aligned} \quad (12)$$

The physiological-based constraint will be achieved by minimizing the magnitude of both $r_u(s, t; \theta_{NN})$ and $r_v(s, t; \theta_{NN})$. Thus, the electrophysiological model-based loss is defined as

$$\mathcal{L}_f = \frac{1}{N_f} \sum_{i=1}^{N_f} ((r_u(s_i, t_i; \theta_{NN}))^2 + (r_v(s_i, t_i; \theta_{NN}))^2) \quad (13)$$

where N_f denotes the total number of selected spatiotemporal collocation points to incorporate the AP model. The physics-based loss combines the effect from both the boundary condition and the electrophysiological model, i.e., $\mathcal{L}_{ph} = \mathcal{L}_{bc} + \mathcal{L}_f$, which is encoded to the DNN loss function to respect the underlying physics laws in inverse ECG modeling.

In order to compute the loss function during the DNN training, it is necessary to acquire the value of partial derivatives of $u(s, t)$ and $v(s, t)$ with respect to spatial or temporal variables. This can be easily achieved through automatic differentiation, which is able to yield the exact result of derivatives without approximation error (except for the round-off error) [38]. Automatic differentiation currently is the most popular method to train the deep neural networks by calculating the derivatives *via* breaking down the differentials in multiple paths using the chain rule. In this study, automatic differentiation is engaged to obtain the derivatives with respect to the spatiotemporal coordinates $[s, t]$ in order to encode the physical laws in the form of a partial differential equation into the DNN.

D. Gaussian Process-based Active Learning for Selecting the Optimal Regularization Parameter

The performance of the proposed P-DL framework also depends on the value of the regularization parameter w , as shown in Eq. (8). In traditional regularization methods, the regularization parameter is generally selected according to the L-curve method [50], which is ambiguous, insecure, and requires solving the inverse ECG problem repeatedly given different parameter values. This may incur a huge computation burden for large-scale inverse ECG modeling. Here, we propose to actively search for the optimal regularization parameter through the Gaussian Process (GP)-based surrogate modeling.

GP has been widely used in machine learning as a method for solving complex black-box optimization problems [51]. Here, we propose a GP-based active learning strategy to search for the optimal regularization parameter. Before establishing the GP active-learning procedure, we first define a balance metric as the criterion to evaluate the prediction performance given the regularization parameter w as

$$m(w) = \log \left[\left(\frac{\mathcal{L}_{hb}}{\mathcal{L}_{ph}} + \frac{\mathcal{L}_{ph}}{\mathcal{L}_{hb}} \right) \cdot \mathcal{L}^2(\theta_{NN}) \right] \quad (14)$$

minimizing of which helps to balance between the physics-based loss \mathcal{L}_{hb} and the data-driven loss \mathcal{L}_f as well as to reduce the value of the overall DNN loss $\mathcal{L}(\theta_{NN})$. As such, the input of the GP modeling is the regularization parameter, i.e., w 's, and the output is the corresponding balance metric, i.e., $m(w)$'s. In the GP modeling, we assume

$$m(w) = \hat{m}(w) + \delta, \quad \delta \sim \mathcal{N}(0, \sigma_\delta^2) \quad (15)$$

where δ is Gaussian white noise added for numerical stability, and $\hat{m}(w)$ is further modeled as a GP, i.e., $\hat{m}(w) \sim \mathcal{GP}(0, \mathcal{K})$, where \mathcal{K} denotes the kernel function which is selected as the widely used square-exponential kernel in the present investigation, i.e.,

$$\mathcal{K}(w_i, w_j) = \sigma_m^2 \cdot \exp\left(-\frac{\|w_i - w_j\|^2}{2l^2}\right) \quad (16)$$

where σ_m and l denote the GP hyperparameters, which can be determined by maximizing the log marginal likelihood for GP regression [52]. Given the collected observations $\{\mathbf{m}_{1:n}, \mathbf{w}_{1:n}\}$, where $\mathbf{m}_{1:n} = [m_1 \dots m_n]^T$ and $\mathbf{w}_{1:n} = [w_1 \dots w_n]^T$, the predictive distribution of $m(w)$ given an arbitrary unevaluated regularization parameter w_* is

$$P(m(w_*) | \mathbf{m}_{1:n}, \mathbf{w}_{1:n}, w_*) = \mathcal{N}(\mu_n(w_*), \sigma_n^2(w_*)) \quad (17)$$

The predictive mean $\mu_n(w_*)$ and variance $\sigma_n^2(w_*)$ is given as

$$\mu_n(w_*) = \mathcal{K}(w_*, \mathbf{w}_{1:n}) (\mathcal{K}(\mathbf{w}_{1:n}, \mathbf{w}_{1:n}) + \sigma_\delta^2 \mathcal{I})^{-1} \mathbf{m}_{1:n} \quad (18)$$

$$\sigma_n^2(w_*) = \mathcal{K}(w_*, w_*) - \mathcal{K}(w_*, \mathbf{w}_{1:n}) (\mathcal{K}(\mathbf{w}_{1:n}, \mathbf{w}_{1:n}) + \sigma_\delta^2 \mathcal{I})^{-1} \mathcal{K}(\mathbf{w}_{1:n}, w_*) \quad (19)$$

where \mathcal{I} represents an identity matrix with the same dimensionality of $\mathcal{K}(\mathbf{w}_{1:n}, \mathbf{w}_{1:n})$.

With the GP-surrogate modeling, we can evaluate the prediction performance of P-DL given an arbitrary value of w without actually solving the inverse ECG problem. As such, we can intuitively select the optimal parameter by minimizing the GP predictive mean, i.e., $w_{opt} = \arg \min_w \{\mu_n(w)\}$. However, the accuracy of the GP surrogate depends on the quality of the training data $\{\mathbf{m}_{1:n}, \mathbf{w}_{1:n}\}$, which requires an effective strategy to collect the most informative data points. To find a best next query point w_{n+1} in the parameter space for updating GP, a good acquisition function should balance the trade-off between exploitation and exploration. For exploitation, we should maximize the posterior probability to select the points with low predictive mean; for exploration, the points with large predictive variances need to be explored to reduce the estimation uncertainty. As such, we propose an active searching strategy based on GP upper-confidence-bound (GP-UCB) [53] as

$$w_{n+1} = \arg \max_w \{-\mu_n(w) + \beta^{1/2} \sigma_n(w)\} \quad (20)$$

where β is a positive constant that balances between the global search and local optimization.

After the new point w_{n+1} is selected, the P-DL framework will be run to solve the inverse ECG problem and calculate the corresponding balance metric $m(w_{n+1})$ with the new regularization parameter w_{n+1} . When the new input-output pair $\{w_{n+1}, m_{n+1}\}$ becomes available, the GP surrogate will be updated according to:

$$\begin{bmatrix} \mathbf{m}_{1:n} \\ m_{n+1} \end{bmatrix} \sim \mathcal{N}\left(0, \begin{bmatrix} \mathcal{K}(\mathbf{w}_{1:n}, \mathbf{w}_{1:n}) + \sigma_\delta^2 \mathbf{I} & \mathcal{K}(\mathbf{w}_{1:n}, w_{n+1}) \\ \mathcal{K}(w_{n+1}, \mathbf{w}_{1:n}) & \mathcal{K}(w_{n+1}, w_{n+1}) \end{bmatrix}\right) \quad (21)$$

This active-learning procedure is repeatedly evaluated until w converges around a certain point where m is expected to have a minimum value, and the converged value of w will be selected as the optimal regularization parameter.

E. Parallel Computing to Increase Computation Efficiency

In the proposed P-DL method, the DNN parameters (i.e., θ_{NN}) can be estimated by back-propagation algorithms incorporated with optimization methods such as stochastic gradient descent (SGD), adaptive moment estimation (Adam), and other optimization methods. In our work, we engage Adam as the optimizer due to its improved generalization performance [54], [55]. This process involves evaluating the gradients of the loss function at each training point (or collocation point) and updating θ_{NN} iteratively. A large number of collocation points will increase the computational intensity of the training process. Fortunately, an appealing feature of the P-DL method is that computing tasks are much easier to be operated in parallel than traditional inverse ECG modeling. Here, we propose to scale up the P-DL algorithm by effectively harnessing the computing power of multiple processors collaboratively.

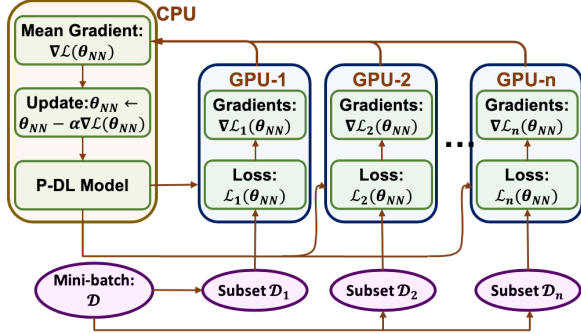


Fig. 2: Scheme for parallel computing.

Fig. 2 shows the proposed strategy for parallel computing. To increase the computational parallelism and escape from the local minima [56], [57], the whole dataset is divided into mini-batch data (denoted as \mathcal{D}), which are further split for the Adam algorithm into n_D subsets during network training, i.e., $\mathcal{D} = \mathcal{D}_1 \cup \mathcal{D}_2 \cup \dots \cup \mathcal{D}_{n_D}$. Thus, the gradient of the loss function with data \mathcal{D} will be calculated as

$$\nabla \mathcal{L}(\theta_{NN}) = \frac{1}{|\mathcal{D}|} [\nabla \mathcal{L}_1(\theta_{NN}) + \dots + \nabla \mathcal{L}_{n_D}(\theta_{NN})] \quad (22)$$

where $\nabla \mathcal{L}_i(\theta_{NN}) = \sum_{j \in \mathcal{D}_i} \nabla \mathcal{L}_i(\theta_{NN})$, denoting the sum of gradients on subset \mathcal{D}_i . As such, parallel computing can be readily implemented to update network hyperparameters by assigning each subset \mathcal{D}_i to an individual processor and combining results from many computing units.

The algorithm is successfully implemented on TensorFlow, which is a popular platform for advanced machine learning, especially for developing deep learning frameworks. TensorFlow can be operated on the heterogeneous environment including a multi-core Central Processing Unit (CPU), Graphic Processing Unit (GPU), and Tensor Processing Unit (TPU)

[58]. Such cutting-edge hardware developments make parallelization applicable, which significantly increases the computation efficiency in the DL training process [59]. In our work, we process the P-DL algorithm on the parallel computing platform NVIDIA CUDA, which is a software framework for programs running across different environments such as CPU and GPU. The neural network is carried on TensorFlow-GPU with Python application programming interface (API), and we found that the computation speed is around 6.5 times faster than running on CPU only.

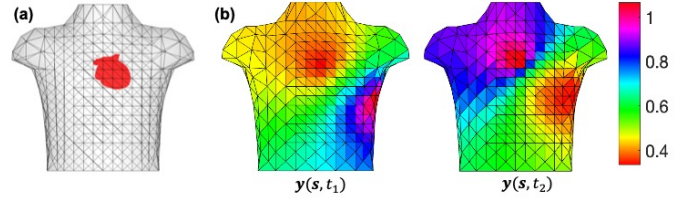


Fig. 3: (a) Illustration of the torso-heart geometry; (b) BSPM at two different time points t_1 and t_2 .

IV. EXPERIMENTAL DESIGN AND RESULTS

We validate and evaluate the performance of the proposed P-DL framework in a 3D torso-heart geometry to estimate the HSP from BSPM measurements. As shown in Fig. 3(a), the heart geometry is formed by 1094 nodes and 2184 mesh elements, and the torso surface consists of 352 nodes and 677 mesh elements, which is obtained from the 2007 PhysioNet Computing in Cardiology Challenge [25], [60]. Fig. 3(b) illustrates the spatiotemporal BSPMs that will be used to predict the HSP. We will investigate the impact of neural network structure, collocation points, noise level, and physics model parameter on the prediction performance as shown in Fig. 4. The proposed P-DL approach will be benchmarked with traditional regularization methods including Tikhonov zero order (Tikh_0th), Tikhonov first order (Tikh_1st), and the spatiotemporal regularization (STRE) (see Eq. (1)-(2) for the objective functions). The model performance will be evaluated according to two metrics: Relative Error (RE) and Correlation Coefficient (CC), which are defined as

$$RE = \frac{\sqrt{\sum_{s,t} \|\hat{\mathbf{u}}(s,t) - \mathbf{u}(s,t)\|^2}}{\sqrt{\sum_{s,t} \|\mathbf{u}(s,t)\|^2}} \quad (23)$$

$$CC = \frac{\sum_s (\hat{\mathbf{u}}(s,\cdot) - \bar{\hat{\mathbf{u}}}(s,\cdot))^T \cdot (\mathbf{u}(s,\cdot) - \bar{\mathbf{u}}(s,\cdot))}{\sum_s \|\hat{\mathbf{u}}(s,\cdot) - \bar{\hat{\mathbf{u}}}(s,\cdot)\| \cdot \|\mathbf{u}(s,\cdot) - \bar{\mathbf{u}}(s,\cdot)\|} \quad (24)$$

where $\mathbf{u}(s,t)$ and $\hat{\mathbf{u}}(s,t)$ represent the reference and estimated HSPs, $\hat{\mathbf{u}}(s,\cdot)$ and $\mathbf{u}(s,\cdot)$ denote the estimated and reference time series vectors at spatial location s , and $\bar{\hat{\mathbf{u}}}(s,\cdot)$ and $\bar{\mathbf{u}}(s,\cdot)$ are the mean of $\hat{\mathbf{u}}(s,\cdot)$ and $\mathbf{u}(s,\cdot)$, respectively.

A. The Impact of Neural Network Structure on the Prediction Performance

In the present investigation, we study the impact of network structure on the prediction performance of the proposed P-DL

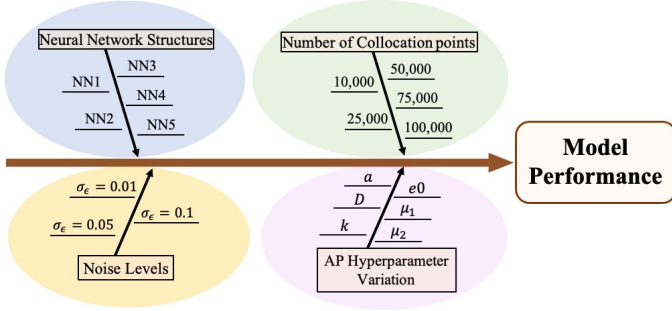


Fig. 4: Experimental design for evaluating the performance of the proposed P-DL approach.

method. Specifically, five feedforward fully-connected neural network structures are evaluated, whose structure details are listed in Table I. Each network structure is evaluated by executing P-DL with the same data input and hyperparameters. Note that a Gaussian noise $\epsilon(s, t) \sim \mathcal{N}(0, \sigma_\epsilon^2)$ with standard deviation $\sigma_\epsilon = 0.01$ is added to BSPM data $y(s, t)$. GP-UCB algorithm is first implemented to find the best regularization parameter to balance between \mathcal{L}_{hb} and \mathcal{L}_{ph} . The active searching procedure is iterated 20 times, and the converged optimal value is obtained as $w^* = 0.44$.

TABLE I: Structure details of different neural networks

	NN1	NN2	NN3	NN4	NN5
Layers	5	3	5	8	5
Neurons	5	10	10	10	20

Fig. 5(a) and (b) shows the RE and CC , respectively, for different structures. Note that the experiments are repeated 10 times for each network structure, and therefore every obtained RE and CC comes with a corresponding error bar (i.e., one standard deviation of RE and CC). The neural network being too thin (e.g., NN1 with 5 neurons for each layer) or too shallow (e.g., NN2 consists of only 3 layers) may cause relatively high RE with a value of (0.2084 ± 0.0188) or (0.1839 ± 0.0052) respectively and low CC value of (0.9641 ± 0.0064) or (0.9722 ± 0.0016) . Thus, a more complex structure is preferred in terms of prediction performance. If we increase the number of neurons in each layer (e.g., NN3 and NN5), or add more layers to the network (e.g., NN4), the resulted RE is significantly reduced. According to Fig.5 (a-b), there is no significant difference among the RE and CC 's obtained from P-DL with NN3, NN4, and NN5, indicating further increasing the network complexity may not be necessary. As such, we choose NN3 as the neural network structure for the later numerical experiments.

B. The Impact of Collocation Points on the Prediction Performance

To enforce the physics laws imposed by the AP model and boundary condition, we need to randomly select an appropriate amount of collocation points from the heart geometry. In the

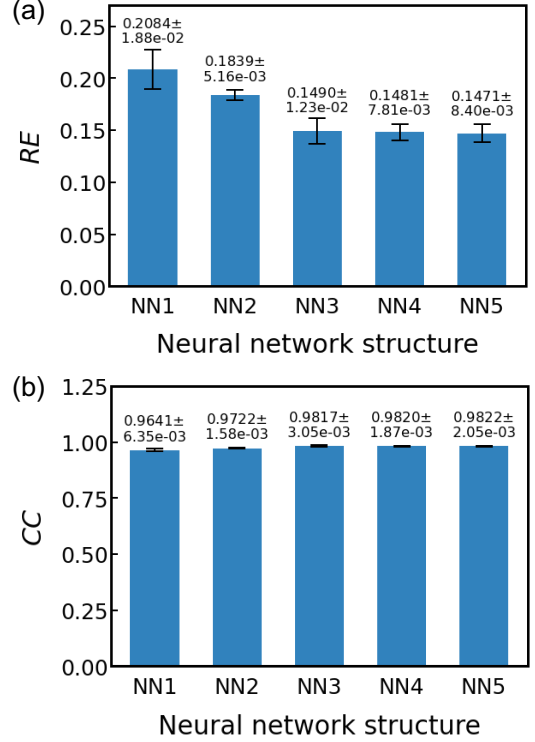


Fig. 5: The variation of (a) RE and (b) CC with respect to neural network structures.

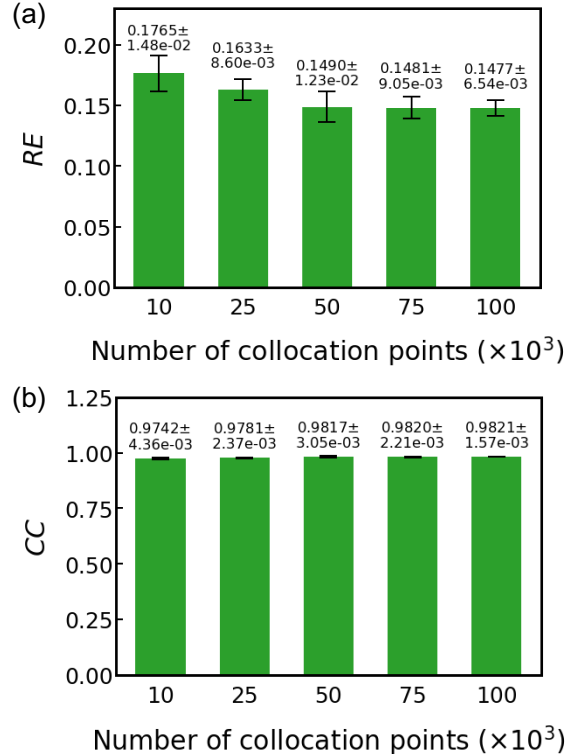


Fig. 6: The variation of (a) RE and (b) CC with respect to the number of collocation points.

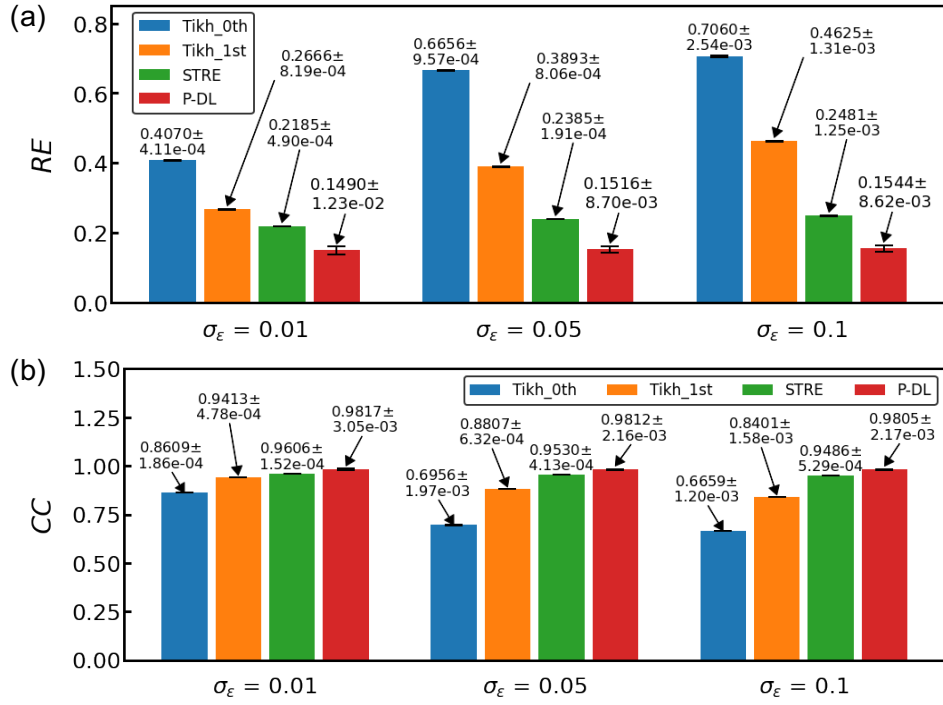


Fig. 7: The comparison of (a) RE and (b) CC between the proposed P-DL method and other regularization models (i.e., Tikh_0th, Tikh_1st, and STRE) in the 3D torso-heart system when different noise levels $\sigma_\epsilon = 0.01, 0.05, 0.1$ are added to the BSPM data $\mathbf{y}(s, t)$.

present investigation, we select five numbers of collocation points: $N_{ph} = 10000, 25000, 50000, 75000, 100000$ to quantify its impact on the predictive accuracy of the proposed P-DL framework. As shown in Fig. 6(a) and (b), the RE decreases and CC increases as we raise the number of collocation points. Specifically, with $N_{ph} = 10000$, the RE is relatively big with a value of (0.1765 ± 0.0148) and the corresponding CC has a comparatively small value of (0.9742 ± 0.0044) , which is due to the fact that the physics principle is insufficiently represented in the overall spatiotemporal domain with such a small number of collocation points. By increasing N_{ph} to 50000, RE is reduced to (0.1490 ± 0.0123) and CC increases to (0.9817 ± 0.0031) . If we continue increasing the number of collocation points, the estimated RE and CC do not improve significantly, besides it may potentially increase the computational burden. Therefore, we select 50000 collocation points for later numerical experiments.

C. Comparison Study with Traditional Regularization Methods

We further benchmark the proposed P-DL framework with traditional regularization methods that are commonly used in current practice (i.e., Tikh_0th, Tikh_1st, and STRE). Fig. 7 (a-b) shows the comparison of RE and CC obtained from the four methods at different noise levels of $\sigma_\epsilon = 0.01, 0.05$, and 0.1 . As the noise level increases from $\sigma_\epsilon = 0.01$ to $\sigma_\epsilon = 0.1$, the RE increases monotonically for all the methods. Specifically, RE increases from (0.4070 ± 0.0004) to (0.7060 ± 0.0025) for Tikh_0th, from (0.2666 ± 0.0008) to (0.4625 ± 0.0013)

for Tikh_1st, from (0.2185 ± 0.0005) to (0.2481 ± 0.0013) for STRE, and from (0.1490 ± 0.0123) to (0.1544 ± 0.0086) for our P-DL model. Correspondingly, CC decreases for each method as the noise level is raised up to $\sigma_\epsilon = 0.1$. Overall, the proposed P-DL model generates the smallest RE and highest CC compared to other regularization methods regardless of the noise level.

As illustrated in Fig. 7 (a-b), it is also worth noting that the estimated RE obtained from the commonly used Tikh_0th and Tikh_1st methods increases dramatically as bigger noises being added to BSPM data $\mathbf{y}(s, t)$, where the RE reaches a 73.4% and 73.5% growth as the noise level increases from $\sigma_\epsilon = 0.01$ to $\sigma_\epsilon = 0.1$, respectively. The STRE model reduces the effect of noise level but still yields an increase level of 13.5%. On the other hand, the proposed P-DL method achieves only a 3.6% increase in RE as the noise level reaches $\sigma_\epsilon = 0.1$. Similarly, CC drops 26.7%, 10.7%, and 1.2% for Tikh_0th, Tikh_1st, and STRE model, whereas for P-DL model, CC only declines by 0.12% as the noise level grows from $\sigma_\epsilon = 0.01$ to $\sigma_\epsilon = 0.1$, exhibiting extraordinary anti-noise performance. Thus, P-DL model not only accomplishes superior prediction accuracy, but also demonstrates the predictive robustness when encountering a high level of noise in BSPM.

Fig. 8(a) delineates the true potential mappings on the heart surface. Because the potential distribution is changing over time dynamically, Fig. 8 only depicts the mappings at one specific time step, i.e., $t = 30$. Note that the HSP $\mathbf{u}(s, t)$ is normalized, and both u and t are unitless. Fig. 8(b-d) show

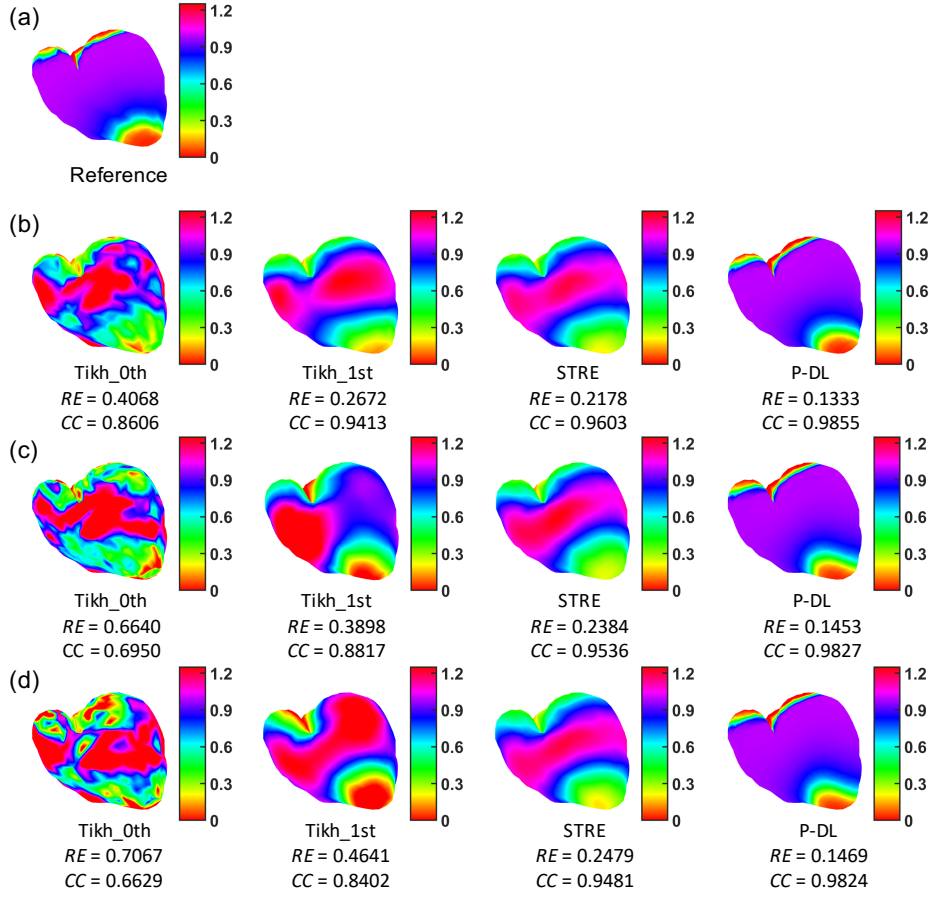


Fig. 8: (a) Reference potential mapping $u(s, t)$ on the heart surface at $t = 30$; Estimated potential mappings $u(s, t)$ at $t = 30$ by P-DL method and other traditional regularization methods (i.e., Tikh_0th, Tikh_1st, and STRE) with noise level of (b) $\sigma_\epsilon = 0.01$ (c) $\sigma_\epsilon = 0.05$ and (d) $\sigma_\epsilon = 0.1$ in BSPM $y(s, t)$.

the estimated HSP distribution generated by the four different methods, with noise level of $\sigma_\epsilon = 0.01$, 0.05 , and 0.1 added to BSPMs $y(s, t)$, respectively. The estimated potential mappings by Tikh_0th, Tikh_1st, and STRE under each noise level present significantly different color patterns compared with the reference mapping in Fig. 8(a). Typically, under the noise level as large as $\sigma_\epsilon = 0.1$, the proposed P-DL yields the RE of 0.1469 , which is remarkably lower than RE estimated by other traditional regularization methods, i.e., 0.7067 by Tikh_0th, 0.4641 by Tikh_1st, 0.2479 by STRE, leading to a similar HSP pattern with the ground truth shown in Fig. 8(a). Similarly, the P-DL model generates the highest CC of 0.9824 , compared to CC value of 0.6629 , 0.8402 , and 0.9481 estimated by Tikh_0th, Tikh_1st, and STRE, respectively, indicating P-DL model yields the smallest pattern difference with the real potential distribution. This is due to the fact that the P-DL model successfully incorporates the bio-electrical propagation (i.e., AP model) and boundary condition, yielding a robust inverse ECG solution.

Furthermore, Fig. 9 shows the comparison of estimated HSPs $\hat{u}(s, t)$ evolving over time for one specific spatial location on the heart geometry given by the four different methods under different noise levels. Note that both Tikh_0th

and Tikh_1st generate noisy estimation whose noisy pattern becomes more significant when σ_ϵ increases from 0.01 to 0.1 . The STRE method smoothens out the noise over time in the estimated signal due to the imposed extra temporal regularization, but the estimated HSP does not reflect the cardiac electrodynamics, leading to a morphology deviation from the true HSP signal. In contrast, by incorporating the physics-based cardiac principles, our proposed P-DL model yields a smooth and robust estimation which matches the morphology pattern of the true HSP signal well under all the three noise levels as illustrated in Fig. 9(a-c).

D. The Impact of Electrophysiological Model Parameters on the Prediction Performance

In the case that AP model could not precisely describe the underlying cardiac electrodynamics, it is necessary to investigate how the variations in the model parameters will influence the predictive accuracy of P-DL model. Table II lists the RE and CC when the individual hyperparameter (i.e., a , k , D , $e0$, μ_1 , μ_2) deviates from the reference value by $\pm 10\%$, given that a noise level of $\sigma_\epsilon = 0.01$ is added to BSPM $y(s, t)$. Note that RE and CC evaluated with the reference parameter setting (i.e., $a = 0.1$, $D = 10$, $k = 8$, $e0 = 0.002$,

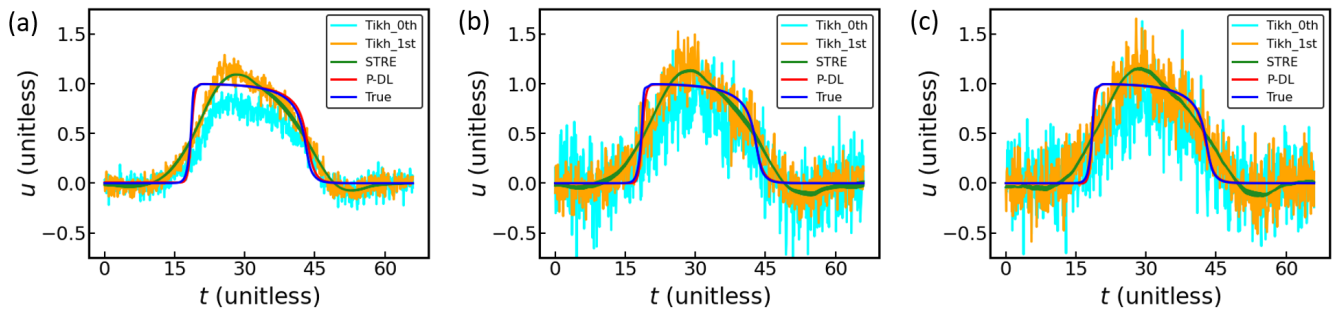


Fig. 9: The comparison of HSP evolution $u(s, t)$ over time for one specific spatial location, between true HSP data and predictions by Tikh_0th, Tikh_1st, STRE, and P-DL under the noise level of (a) $\sigma_\epsilon = 0.01$, (b) $\sigma_\epsilon = 0.05$, (c) $\sigma_\epsilon = 0.1$.

TABLE II: The influence of variations in AP model parameters ($\pm 10\%$) on the RE and CC provided by the P-DL method.

		a	k	D	$e0$	μ_1	μ_2
RE	-10%	0.1681	0.1525	0.1665	0.1620	0.1625	0.1777
	+10%	0.1550	0.1797	0.1647	0.1615	0.1949	0.1701
CC	-10%	0.9768	0.9809	0.9773	0.9785	0.9783	0.9742
	+10%	0.9804	0.9738	0.9778	0.9786	0.9690	0.9763

$\mu_1 = \mu_2 = 0.3$) is (0.1490 ± 0.0123) and (0.9817 ± 0.0031) as shown in Fig. 7.

After designated $\pm 10\%$ variations to the AP parameters, the overall prediction performance deteriorates with an increase in RE and a decrease in CC . Nevertheless, as shown in Table II, RE predicted by the proposed P-DL model with $\pm 10\%$ variations in the AP hyperparameters still rank the smallest compared with other regularization methods with true AP hyperparameter settings, i.e., (0.4070 ± 0.0004) by Tikh_0th, (0.2666 ± 0.0008) by Tikh_1st, and (0.2185 ± 0.0005) by STRE. Similarly, the CC estimated by P-DL method scores the highest value among the four methods, i.e., (0.8609 ± 0.0002) by Tikh_0th, (0.9413 ± 0.0005) by Tikh_1st, and (0.9606 ± 0.0002) by STRE even when the model is provided with an inaccurate AP parameters. Although the AP model with imperfect parameter setting is encoded as the physics constraint into the P-DL model, the body-heart transformation loss \mathcal{L}_{hb} also plays an important role in optimizing the neural network. These two parts interact with each other, making the P-DL model robust against the measurement noises and parameter uncertainties.

V. CONCLUSIONS

In this paper, we propose a physics-constrained deep learning (P-DL) strategy for modeling the dynamic evolution of cardiac electrical potential and predict the heart-surface electrical signals from body-surface sensor measurements. First, we encode the underlying physics law of cardiac electrodynamics into a DNN to solve the inverse ECG model. Second, in order to balance between the body-heart transformation (i.e., data-driven loss) and physics-based loss, we defined a balance metric as an indicator to evaluate the predictive performance given different regularization parameters. Third, we develop an active-learning strategy based on GP-UCB to search for the optimal regularization parameter. Finally, we propose to im-

plement the P-DL with TensorFlow-GPU to increase the computation efficiency. We validate and evaluate the performance of the P-DL framework in a 3D torso-heart system to estimate HSP from BSPM data. Numerical experiments demonstrate that the proposed P-DL model is robust against measurement noises and other uncertainty factors. The inverse ECG solution by the P-DL methods significantly outperforms the traditional regularization methods, i.e., Tikhonov zero-order, Tikhonov first-order, and STRE model that are commonly used in current practice. The presented P-DL framework can be broadly implemented to investigate other spatiotemporal high-dimensional systems such as thermodynamics and tumor-growth systems.

REFERENCES

- [1] H. S. Oster, B. Taccardi, R. L. Lux, P. R. Ershler, and Y. Rudy, "Electrocardiographic imaging: noninvasive characterization of intramural myocardial activation from inverse-reconstructed epicardial potentials and electrograms," *Circulation*, vol. 97, no. 15, pp. 1496–1507, 1998.
- [2] H. Yang, C. Kan, G. Liu, and Y. Chen, "Spatiotemporal differentiation of myocardial infarctions," *IEEE Transactions on Automation Science and Engineering*, vol. 10, no. 4, pp. 938–947, 2013.
- [3] N. Herring and D. Paterson, "Ecg diagnosis of acute ischaemia and infarction: past, present and future," *Journal of the Association of Physicians*, vol. 99, no. 4, pp. 219–230, 2006.
- [4] R. R. Bond, D. D. Finlay, C. D. Nugent, and G. Moore, "Xml-bspm: an xml format for storing body surface potential map recordings," *BMC Medical Informatics and Decision Making*, vol. 10, no. 1, p. 28, 2010.
- [5] D. Lacroix, M. Dubuc, T. Kus, P. Savard, M. Shenasa, and R. Nadeau, "Evaluation of arrhythmic causes of syncope: correlation between holter monitoring, electrophysiologic testing, and body surface potential mapping," *American heart journal*, vol. 122, no. 5, pp. 1346–1354, 1991.
- [6] Y. Rudy and J. E. Burnes, "Noninvasive electrocardiographic imaging," *Annals of Noninvasive electrocardiology*, vol. 4, no. 3, pp. 340–359, 1999.
- [7] Y. Chen and H. Yang, "Sparse modeling and recursive prediction of space-time dynamics in stochastic sensor networks," *IEEE Transactions on Automation Science and Engineering*, vol. 13, no. 1, pp. 215–226, 2015.

- [8] S. Piri, D. Delen, T. Liu, and H. M. Zolbanin, "A data analytics approach to building a clinical decision support system for diabetic retinopathy: Developing and deploying a model ensemble," *Decision Support Systems*, vol. 101, pp. 12–27, 2017.
- [9] Y. Lin, S. Liu, and S. Huang, "Selective sensing of a heterogeneous population of units with dynamic health conditions," *IJSE Transactions*, vol. 50, no. 12, pp. 1076–1088, 2018.
- [10] B. Si, I. Yakushev, and J. Li, "A sequential tree-based classifier for personalized biomarker testing of alzheimer's disease risk," *IJSE Transactions on Healthcare Systems Engineering*, vol. 7, no. 4, pp. 248–260, 2017.
- [11] B. Yao, R. Zhu, and H. Yang, "Characterizing the location and extent of myocardial infarctions with inverse ecg modeling and spatiotemporal regularization," *IEEE journal of biomedical and health informatics*, vol. 22, no. 5, pp. 1445–1455, 2017.
- [12] A. S. Iquebal and S. T. Bukkapatnam, "Consistent estimation of the max-flow problem: Towards unsupervised image segmentation," *IEEE Transactions on Pattern Analysis and Machine Intelligence*, 2020.
- [13] B. Yao, Y. Chen, and H. Yang, "Constrained markov decision process modeling for optimal sensing of cardiac events in mobile health," *IEEE Transactions on Automation Science and Engineering*, pp. 1–13, 2021.
- [14] J. Corral-Acero, F. Margara, M. Marciniak, C. Rodero, F. Loncaric, Y. Feng, A. Gilbert, J. F. Fernandes, H. A. Bukhari, A. Wajdan *et al.*, "The 'digital twin' to enable the vision of precision cardiology," *European heart journal*, vol. 41, no. 48, pp. 4556–4564, 2020.
- [15] N. Trayanova, "From genetics to smart watches: developments in precision cardiology," *Nature Reviews Cardiology*, vol. 16, no. 2, pp. 72–73, 2019.
- [16] H. S. Oster, B. Taccardi, R. L. Lux, P. R. Ershler, and Y. Rudy, "Noninvasive electrocardiographic imaging: reconstruction of epicardial potentials, electrograms, and isochrones and localization of single and multiple electrocardiac events," *Circulation*, vol. 96, no. 3, pp. 1012–1024, 1997.
- [17] R. M. Gulrajani, "The forward and inverse problems of electrocardiography," *IEEE Engineering in Medicine and Biology Magazine*, vol. 17, no. 5, pp. 84–101, 1998.
- [18] B. Yao and H. Yang, "Spatiotemporal regularization for inverse ecg modeling," *IJSE Transactions on Healthcare Systems Engineering*, pp. 1–13, 2020.
- [19] D. H. Brooks, G. F. Ahmad, R. S. MacLeod, and G. M. Maratos, "Inverse electrocardiography by simultaneous imposition of multiple constraints," *IEEE Transactions on Biomedical Engineering*, vol. 46, no. 1, pp. 3–18, 1999.
- [20] F. Greensite, "The temporal prior in bioelectromagnetic source imaging problems," *IEEE transactions on biomedical engineering*, vol. 50, no. 10, pp. 1152–1159, 2003.
- [21] L. Wang, H. Zhang, K. C. Wong, H. Liu, and P. Shi, "Physiological-model-constrained noninvasive reconstruction of volumetric myocardial transmembrane potentials," *IEEE Transactions on Biomedical Engineering*, vol. 57, no. 2, pp. 296–315, 2009.
- [22] L. Yu, Z. Zhou, and B. He, "Temporal sparse promoting three dimensional imaging of cardiac activation," *IEEE transactions on medical imaging*, vol. 34, no. 11, pp. 2309–2319, 2015.
- [23] A. Karoui, L. Bear, P. Migerditchan, and N. Zemzemi, "Evaluation of fifteen algorithms for the resolution of the electrocardiography imaging inverse problem using ex-vivo and in-silico data," *Frontiers in physiology*, vol. 9, p. 1708, 2018.
- [24] R. C. Barr, M. Ramsey, and M. S. Spach, "Relating epicardial to body surface potential distributions by means of transfer coefficients based on geometry measurements," *IEEE Transactions on biomedical engineering*, no. 1, pp. 1–11, 1977.
- [25] F. Dawoud, G. S. Wagner, G. Moody, and B. M. Horáček, "Using inverse electrocardiography to image myocardial infarction—reflecting on the 2007 physionet/computers in cardiology challenge," *Journal of electrocardiology*, vol. 41, no. 6, pp. 630–635, 2008.
- [26] D. Wang, R. M. Kirby, and C. R. Johnson, "Finite-element-based discretization and regularization strategies for 3-d inverse electrocardiography," *IEEE Transactions on Biomedical Engineering*, vol. 58, no. 6, pp. 1827–1838, 2011.
- [27] R. D. Throne and L. G. Olson, "Fusion of body surface potential and body surface laplacian signals for electrocardiographic imaging," *IEEE Transactions on biomedical engineering*, vol. 47, no. 4, pp. 452–462, 2000.
- [28] S. Ghosh and Y. Rudy, "Application of l1-norm regularization to epicardial potential solution of the inverse electrocardiography problem," *Annals of biomedical engineering*, vol. 37, no. 5, pp. 902–912, 2009.
- [29] G. Shou, L. Xia, F. Liu, M. Jiang, and S. Crozier, "On epicardial potential reconstruction using regularization schemes with the l1-norm data term," *Physics in Medicine & Biology*, vol. 56, no. 1, p. 57, 2010.
- [30] B. Messnarz, B. Tilg, R. Modre, G. Fischer, and F. Hanser, "A new spatiotemporal regularization approach for reconstruction of cardiac transmembrane potential patterns," *IEEE transactions on Biomedical Engineering*, vol. 51, no. 2, pp. 273–281, 2004.
- [31] B. Yao and H. Yang, "Physics-driven spatiotemporal regularization for high-dimensional predictive modeling: A novel approach to solve the inverse ecg problem," *Scientific reports*, vol. 6, no. 1, pp. 1–13, 2016.
- [32] Y. LeCun, Y. Bengio, and G. Hinton, "Deep learning," *nature*, vol. 521, no. 7553, pp. 436–444, 2015.
- [33] R. A. Houser, S. D. Edwards, and T. F. Kordis, "Catheters and methods for performing cardiac diagnosis and treatment," May 24 1994, uS Patent 5,313,943.
- [34] M. Raissi, P. Perdikaris, and G. E. Karniadakis, "Physics-informed neural networks: A deep learning framework for solving forward and inverse problems involving nonlinear partial differential equations," *Journal of Computational Physics*, vol. 378, pp. 686–707, 2019.
- [35] Y. Zhu, N. Zabarar, P.-S. Koutsourelakis, and P. Perdikaris, "Physics-constrained deep learning for high-dimensional surrogate modeling and uncertainty quantification without labeled data," *Journal of Computational Physics*, vol. 394, pp. 56–81, 2019.
- [36] X. Jia, J. Willard, A. Karpatne, J. S. Read, J. A. Zwart, M. Steinbach, and V. Kumar, "Physics-guided machine learning for scientific discovery: An application in simulating lake temperature profiles," *arXiv preprint arXiv:2001.11086*, 2020.
- [37] X. Jin, S. Cai, H. Li, and G. E. Karniadakis, "Nsfnets (navier-stokes flow nets): Physics-informed neural networks for the incompressible navier-stokes equations," *arXiv preprint arXiv:2003.06496*, 2020.
- [38] C. Rao, H. Sun, and Y. Liu, "Physics informed deep learning for computational elastodynamics without labeled data," *arXiv preprint arXiv:2006.08472*, 2020.
- [39] X. Chen, X. Chen, W. Zhou, J. Zhang, and W. Yao, "The heat source layout optimization using deep learning surrogate modeling," *Structural and Multidisciplinary Optimization*, vol. 62, no. 6, pp. 3127–3148, 2020.
- [40] J. Sun, J. Zhang, X. Zhang, and W. Zhou, "A deep learning-based method for heat source layout inverse design," *IEEE Access*, vol. 8, pp. 140 038–140 053, 2020.
- [41] H. Mao, "Integrated cardiac electromechanics: Modeling and personalization," 2015.
- [42] M. Sermesant, H. Delingette, and N. Ayache, "An electromechanical model of the heart for image analysis and simulation," *IEEE transactions on medical imaging*, vol. 25, no. 5, pp. 612–625, 2006.
- [43] O. Camara, M. Sermesant, P. Lamata, L. Wang, M. Pop, J. Relan, M. De Craene, H. Delingette, H. Liu, S. Niederer *et al.*, "Inter-model consistency and complementarity: Learning from ex-vivo imaging and electrophysiological data towards an integrated understanding of cardiac physiology," *Progress in Biophysics and Molecular Biology*, vol. 107, no. 1, pp. 122–133, 2011.
- [44] R. R. Aliev and A. V. Panfilov, "A simple two-variable model of cardiac excitation," *Chaos, Solitons & Fractals*, vol. 7, no. 3, pp. 293–301, 1996.
- [45] R. Collobert and J. Weston, "A unified architecture for natural language processing: Deep neural networks with multitask learning," in *Proceedings of the 25th international conference on Machine learning*, 2008, pp. 160–167.
- [46] S. Hijazi, R. Kumar, and C. Rowen, "Using convolutional neural networks for image recognition," *Cadence Design Systems Inc.: San Jose, CA, USA*, pp. 1–12, 2015.
- [47] W. Yang, L. Jin, D. Tao, Z. Xie, and Z. Feng, "DropSample: A new training method to enhance deep convolutional neural networks for large-scale unconstrained handwritten chinese character recognition," *Pattern Recognition*, vol. 58, pp. 190–203, 2016.
- [48] B. Kehoe, S. Patil, P. Abbeel, and K. Goldberg, "A survey of research on cloud robotics and automation," *IEEE Transactions on automation science and engineering*, vol. 12, no. 2, pp. 398–409, 2015.
- [49] J. Wang, Y. Ma, L. Zhang, R. X. Gao, and D. Wu, "Deep learning for smart manufacturing: Methods and applications," *Journal of Manufacturing Systems*, vol. 48, pp. 144–156, 2018.
- [50] P. C. Hansen and D. P. O'Leary, "The use of the l-curve in the regularization of discrete ill-posed problems," *SIAM journal on scientific computing*, vol. 14, no. 6, pp. 1487–1503, 1993.
- [51] M. Seeger, "Gaussian processes for machine learning," *International journal of neural systems*, vol. 14, no. 02, pp. 69–106, 2004.
- [52] C. E. Rasmussen, "Gaussian processes in machine learning," in *Summer School on Machine Learning*. Springer, 2003, pp. 63–71.

- [53] N. Srinivas, A. Krause, S. M. Kakade, and M. W. Seeger, "Information-theoretic regret bounds for gaussian process optimization in the bandit setting," *IEEE Transactions on Information Theory*, vol. 58, no. 5, pp. 3250–3265, 2012.
- [54] N. S. Keskar and R. Socher, "Improving generalization performance by switching from adam to SGD," *arXiv preprint arXiv:1712.07628*, 2017.
- [55] D. P. Kingma and J. Ba, "Adam: A method for stochastic optimization," *arXiv preprint arXiv:1412.6980*, 2014.
- [56] L. Bottou, "Large-scale machine learning with stochastic gradient descent," in *Proceedings of COMPSTAT'2010*. Springer, 2010, pp. 177–186.
- [57] R. Ge, F. Huang, C. Jin, and Y. Yuan, "Escaping from saddle points—online stochastic gradient for tensor decomposition," in *Conference on Learning Theory*, 2015, pp. 797–842.
- [58] M. Abadi, P. Barham, J. Chen, Z. Chen, A. Davis, J. Dean, M. Devin, S. Ghemawat, G. Irving, M. Isard *et al.*, "Tensorflow: A system for large-scale machine learning," in *12th {USENIX} symposium on operating systems design and implementation ({OSDI} 16)*, 2016, pp. 265–283.
- [59] S. Shi, Q. Wang, P. Xu, and X. Chu, "Benchmarking state-of-the-art deep learning software tools," in *2016 7th International Conference on Cloud Computing and Big Data (CCBD)*. IEEE, 2016, pp. 99–104.
- [60] A. L. Goldberger, L. A. Amaral, L. Glass, J. M. Hausdorff, P. C. Ivanov, R. G. Mark, J. E. Mietus, G. B. Moody, C.-K. Peng, and H. E. Stanley, "Physiobank, physiotoolkit, and physionet: components of a new research resource for complex physiologic signals," *circulation*, vol. 101, no. 23, pp. e215–e220, 2000.